Acta Astronautica 91 (2013) 322–332

Contents lists available at SciVerse ScienceDirect

Acta Astronautica

journal homepage: www.elsevier.com/locate/actaastro

# Inflatable antenna for cubesats: Motivation for development and antenna design ☆

Alessandra Babuscia [a,*], Benjamin Corbin [a], Mary Knapp [a], Rebecca Jensen-Clem [b], Mark Van de Loo [a], Sara Seager [a]

[a] Massachusetts Institute of Technology, USA
[b] California Institute of Technology, USA

ARTICLE INFO

*Article history:*
Received 14 November 2012
Received in revised form
28 May 2013
Accepted 5 June 2013
Available online 19 June 2013

*Keywords:*
CubeSat
Inflatable
Antenna
Communication systems

ABSTRACT

CubeSats and small satellites have potential to provide means to explore space and to perform science in a more affordable way. As the goals for these spacecraft become more ambitious in space exploration, moving from Low Earth Orbit (LEO) to Geostationary Earth Orbit (GEO) or further, the communication systems currently implemented will not be able to support those missions. One of the bottlenecks in small spacecraft communication systems is represented by antennas' size, due to the close relation between antenna gain and dimensions. Current antennas for CubeSats are mostly dipole or patch antennas with limited gain. Deployable (not inflatable) antennas for CubeSats are currently being investigated, but these solutions are affected by the challenge of packaging the whole deployable structure in a small spacecraft.

The work that we propose represents the first attempt to develop an inflatable antenna for CubeSats. Inflatable structures and antennas can be packaged efficiently occupying a small amount of space, and they can provide, once deployed, large dish dimension and correspondent gain. Inflatable antennas have been previously tested in space (Inflatable Antenna Experiment, STS-77). However they have never been developed for small spacecraft such as CubeSats, where the packaging efficiency, the deployment, and the inflation represent a challenge.

Our study explores for the first time the possibility of developing such antenna in a way compatible with CubeSat dimensions and constraints. The research provides answers on the possible dimensions for an inflatable antenna for small satellites, on the gain and resolution that can be achieved, and on the deployment and inflation mechanism compatible with CubeSat. Future work in the development of the antenna will include the test of the antenna in flight during a specific technical demonstration mission.

The article is structured as follows: context and motivation for Cubesat inflatable antenna are described; then a study to design the antenna which achieves the required performance metrics, while respecting the constraints imposed by CubeSat structure, is presented.



## 1. Introduction

CubeSats and other small satellites have potential to provide means to explore space and to carry out scientific experiments in an affordable way. As missions for these spacecraft become more ambitious, moving from Low

☆ This paper was presented during the 63rd IAC in Naples.

* Corresponding author. Tel.: +1 617 8005219.
*E-mail addresses:* babuscia@mit.edu (A. Babuscia), bcorbin@mit.edu (B. Corbin), mknapp@mit.edu (M. Knapp). rjensen@caltech.edu (R. Jensen-Clem), mvdl@mit.edu (M. Van de Loo). seager@mit.edu (S. Seager).

0094-5765/$ - see front matter © 2013 IAA. Published by Elsevier Ltd. All rights reserved.
http://dx.doi.org/10.1016/j.actaastro.2013.06.005

Earth Orbit (LEO) to Geostationary Earth Orbit (GEO) and beyond, the communication systems currently implemented will no longer be adequate. Current communication systems for the CubeSats platform [1] utilize frequencies ranging from VHF to S-Band, using primarily dipole and patch antennas (peak gain generally limited to 6 dB), and transceivers with limited transmission power (approximately 1 W). These systems are suitable for a satellite located in LEO and for missions with low data rate requirements. However, for future missions that aim to reach farther points in the solar system and to utilize high data rates, new communications solutions must be developed.

Inflatable antennas can provide higher gain than patch antennas or monopoles [1] and they can be stored in a stowed configuration which occupies less space than monolithic dishes. However, they have never been realized in a way compatible with the CubeSat form factor, where packaging efficiency, deployment, and inflation represent a particular challenge.

Research in the area of inflatable structures and specifically inflatable space antennas has been conducted since the 1950s. A preliminary experiment was the NASA Echo Balloons Project, developed in the late 1950s. Echo-I [2] was made from a 12 μm Mylar membrane with vapor-deposited aluminum and it was successfully launched on August 12, 1960. The Echo-I was operational for several months, maintaining its inflated profile. In the 1990s, one inflatable antenna design was tested in space [3–5] during the STS-77 mission (May 1996). The antenna consisted of a 14-meter diameter lenticular reflector structure, connected to the main spacecraft by an inflatable torus and a set of 28-meter struts. The basic antenna support structure (torus and struts) was deployed successfully, but in an uncontrolled manner. A malfunction of the gas inflation system did not allow full inflation of the lenticular reflector structure. Unexpected spacecraft dynamics were observed during deployment due to residual air in the inflatable components.

Other works in the field of inflatable space antennas include the development and testing of inflatable Microstrip Reflectarrays for X-Band and Ka-Band by ILC Dover [6–9]. The X-Band Reflectarray structure includes a 1-meter diameter antenna membrane assembly supported by an inflatable torus. This antenna is designed primarily for radar applications and it is not readily compatible with CubeSat form factor.

Another recent study [10] discusses the structural design of a 3.2-meter inflatable structure. This antenna has been developed and the radiation pattern has been experimentally measured, but the design is difficult to adapt for compatibility with the CubeSat form factor.

Our research represents the first attempt at developing an inflatable antenna for the CubeSat platform. In [11], the authors presented benefits of inflatable antennas and a possible design of the inflatable antenna for CubeSat.

This article is structured as follows: first an overview of the benefits of developing an inflatable antenna for CubeSats is presented. Second, the design of the inflatable antenna and the results of the radiation model are described. Additional aspects of CubeSat design which are important for the project such as attitude and control, power and avionics are briefly discussed. Finally, the plan for the test plan campaign is described.

## 2. Motivation for the development of inflatable antenna for CubeSat

The development of an inflatable antenna for CubeSats will greatly increase the transmitting and receiving gain for an antenna that can be contained in a spacecraft as small as a CubeSat. Specifically, for a 1 m inflatable antenna in the S-Band, the theoric estimated gain (computed assuming an efficiency $\eta=0.5$) is approximately:

$$G=\frac{\pi^2 D^2 \eta}{\lambda^2}\approx 24.9\ \text{dB} \tag{1}$$

This increased gain will allow CubeSats to transmit data at a higher rate and from a farther distance. These two aspects are summarized in the following two subsections. For more details on the analysis and on the results, please refer to [11].

### 2.1. Benefit 1: increases data rate

An increase in gain will allow a correspondent increase in the data rate. A simulation in [11] shows that by using the inflatable antenna, a CubeSat could potentially transmit data at 100 kbps from an orbit close to GEO, while a communication system equipped with a traditional patch antenna would generally reach less than 10 bps of data rate.

### 2.2. Benefit 2: enables interplanetary communication

The increase in gain will also allow a CubeSat to transmit data to the Earth from a further point in the solar system with respect to a CubeSat equipped with traditional patch antennas or dipole. Specifically, from the simulation described in [11], the distance that can be covered by a CubeSat equipped with the inflatable antenna is at least seven times greater than the ones covered by a CubeSat equipped with a microstrip antenna.

## 3. Inflatable antenna design

The antenna is designed for the S-Band and it includes a reflector surface of 1 m in diameter. The next sections detail the configuration, design and fabrication of the first prototype. Additionally, the results of the simulation of the radiation diagram and the different aspects of the spacecraft design are presented.

### 3.1. Antenna configuration, design and fabrication

Fig. 1 shows a concept drawing of the deployed antenna on the back of a 3U Cubesat. A standard patch antenna will beam radio signal from inside the inflated volume onto a parabolic reflective surface. That signal transmits through the other side of the inflated volume, which is transparent, to the target. The inflatable antenna is made from 50.8 μm thick metalized Mylar (PET) on the reflective part and

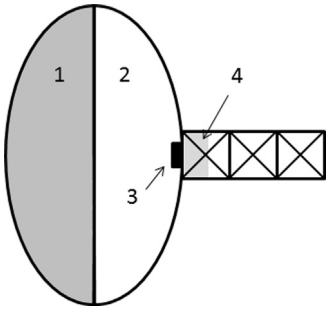


**Fig. 1.** Concept sketch of the inflatable antenna, with reflective Mylar [1], transparent Mylar [2], a patch antenna [3], and a stowed volume of less than 1 μ [4] on a 3U Cubesat.

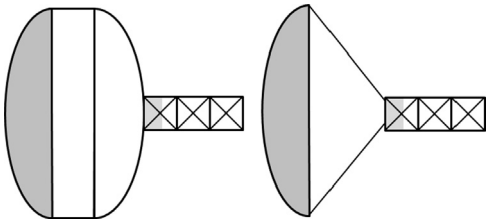

**Fig. 2.** Concept sketches of the cylindrical (left) and conical (right) inflatable antenna configurations. In both cases, the reflector is 1 m wide with a focal length of 0.5 m.

25.4 μm thick transparent Mylar for the rest of the inflatable.

Currently, there are two configurations being considered, one is shaped like a cylinder, the other is shaped like a cone (Fig. 2). Whether the inflatable can hold a parabolic shape in the reflector is still unknown, but several ideas have been proposed to increase the rigidity along the circle that connects the reflective and transparent parts, including memory wire and an inflatable toroid at a higher pressure.

The antenna is inflated using a small amount of sublimating powder placed into the vacuum-packed antenna. When it is deployed, the sublimating powder will turn into a gas and inflate the antenna to a pressure on the order of $10^{-3}$ Torr. Using a passive sublimating powder to inflate the antenna removes the need for active inflation hardware like gas tanks, hoses, and valves, which can be heavy and use up the mass budget. This sublimating powder will continue to inflate the antenna and provide pressure even when leaks are present (see Section 3.3). Currently, benzoic acid is the chosen sublimating powder, but others are being considered depending on their vapour pressure vs. temperature curves.

The parabolic reflector is created by cutting petal-shaped pieces out of the metalized Mylar and combining them to form a curved surface [2]. Fig. 3 shows an example of how a paraboloid can be cut out of a flat sheet using four petals. The edges of the petals are then joined together first with Kapton tape and then with an epoxy specifically designed to connect hard-to-bond plastics like Mylar.

In the cylindrical configuration, an identical paraboloid is made with clear Mylar, and the two paraboloids are connected with a cylindrical piece of clear Mylar. Then, a small hole is cut in the transparent paraboloid so it can be

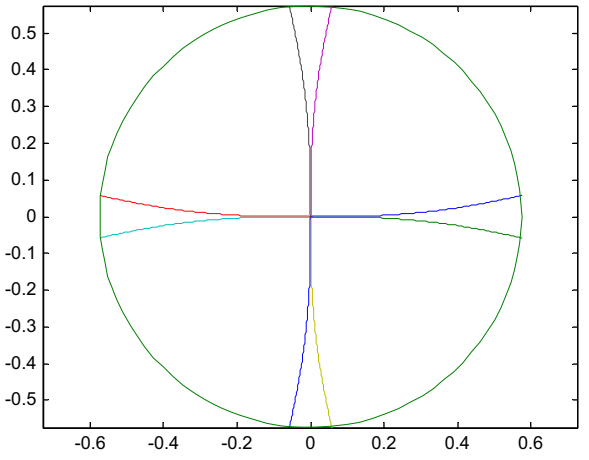


**Fig. 3.** Four-petal flat sheet that, when joined along the edges, forms a 1 m diameter paraboloid with 0.25 m focal length (the smaller focal length used in the figure is only to more clearly illustrate the area cut out of the flat sheet).

bonded to the plate where the patch antenna is secured. In the conical configuration, a cone is made with clear Mylar and bonded directly to the paraboloid. Since the cutting pattern is made to include a hole already, it does not need another one cut in it to be bonded to the plate with the patch antenna.

Vacuum bagging the antenna is essential because left-over air could over-pressurize the balloon and cause it to burst on deployment or deploy prematurely if there is enough to force the locking mechanism open. If a hole cannot be drilled through the patch antenna plate to apply a vacuum, a nipple can be installed at the center of the reflector to vacuum pack the antenna.

Folding and packing the antenna still remains a challenge because wrinkles in the reflective part of the Mylar do not come out easily, and the inflated pressure is low and may not provide the necessary stress to flatten wrinkles. Anechoic chamber testing will include gain tests on both a pristine, unwrinkled version of the antenna and a recently-packed antenna with wrinkle patterns that may be seen after deployment. Vacuum testing will ensure vacuum packing methods do not leave too much air in the inflatable volume as well as show how effective the sublimating powder can be at removing wrinkles.

Additional sensors were considered to be added to the plate the inflatable section mounts to with the patch antenna, such as a small pressure sensor and a camera to capture the deployment process, but because the patch antenna take up most of the space on the plate, it would interfere with the broadcast signal.

There are additional concerns with the fabrication and testing of the antenna with the materials being used. The vapour pressure and outgassing characteristics of the epoxies selected for testing are unknown. As a result, the epoxy will be applied to the outside edges of the inflated volume in case the vapour pressure of the epoxy is higher than the vapour pressure of the sublimating powder. While the outgassing constituents of the materials used in fabrication will not affect radio transmissions like it does in low-wavelength optics, the testing facilities that

are available for this project require high levels of cleanliness; as a result, the materials selection requirements are actually stricter for testing than they are for flight.

### 3.2. Radiation model: simulation of inflatable antenna

The objective of the radiation model is to analyze the previously described inflatable antenna configurations to characterize the effects of the feed selected, of the geometry of the dish, and of the dielectric shape. The radiation model provides answer to the following questions:

- Is the choice of using a microstrip patch antenna as feed appropriate? The results show that the microstrip patch antenna allows the reflector to achieve a sufficiently high gain (peak around 23 dB), and that the spillover losses are limited.
- Does the CubeSat 3U structure placed in the line of sight of the reflector, affect the final radiation diagram? The results show that the CubeSat structure does not affect the radiation diagram.
- Do the dielectric (mylar) and the geometry of the inflatable structure affect the radiation? The analysis shows a reduction of the peak gain of approximately 7 dB if a conical inflatable dielectric shape (Fig. 16) is used. Differently, if the shape of the inflatable dielectric structure is cylindrical, the reduction in the peak gain is only 2 dB (Fig. 18).

Additional aspects that still need to be modelled are the effects due to micrometeoroid impacts, anomalies in the deployment and in the inflation, and thermal variations. The current model does not take into account these effects.

The radiation model is developed using FEKO software [12] and the analysis is performed in different stages. Initially, only the radiation of the microstrip patch antenna is modelled. This initial step is important to fully characterize the feed before studying the effects of the reflector surface. The patch antenna considered is a 9 cm × 9 cm antenna which will fit easily in the CubeSat structure. The characteristic of the antenna are summarized in Table 1. The antenna has been designed to be optimized for 2.4 GHz. The CAD model of the antenna is shown in Fig. 4. The radiation diagram in 3D view at 2.4 GHz is shown in Fig. 5. The polar diagram is shown in Fig. 6. The radiation diagram reveals a rounded radiation shape, typical of the patch antenna with a peak gain (at the desired frequency of 2.4 GHz) of approximately 8 dB.

**Table 1**
Parameters of the customized microstrip patch antenna used as the feed for the parabolic reflector.

| Parameter | Value |
|---|---|
| Central frequency | 2.4 GHz |
| Dielectric surface | 9 cm × 9 cm |
| Dielectric constant | 2.2 |
| Dielectric thickness | 1.57 mm |
| Width of the conductive surface ($w$) | 48.56 mm |
| Length of the conductive surface ($L$) | 39.75 mm |

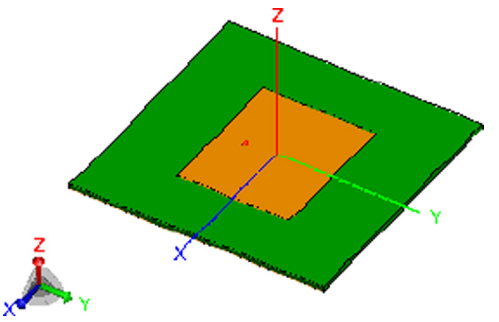


**Fig. 4.** CAD view of the patch antenna.

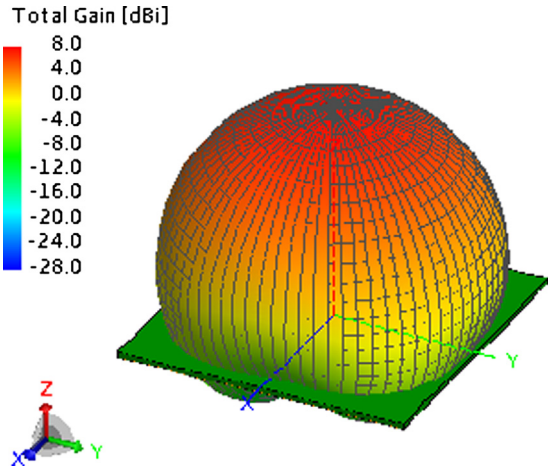


**Fig. 5.** Radiation diagram of the patch antenna (3D view, 2.4 GHz).

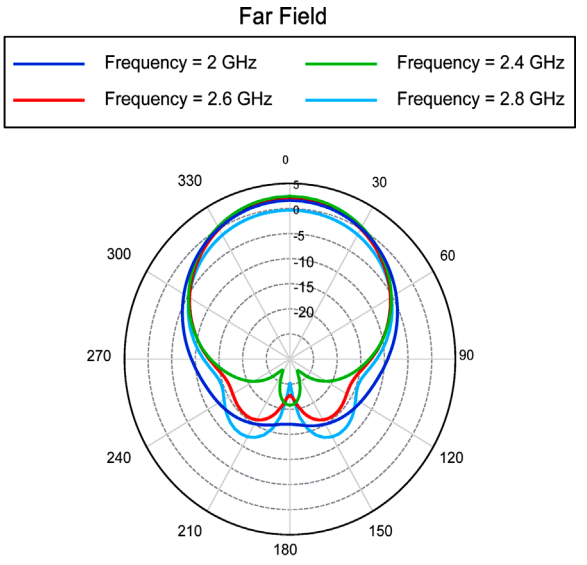


**Fig. 6.** Polar radiation diagram of the patch antenna at different frequencies.

After modelling the patch antenna, the reflector is added. This analysis allows the computation of the gain of the reflector without considering the attenuation imposed by the dielectric or by the presence of the

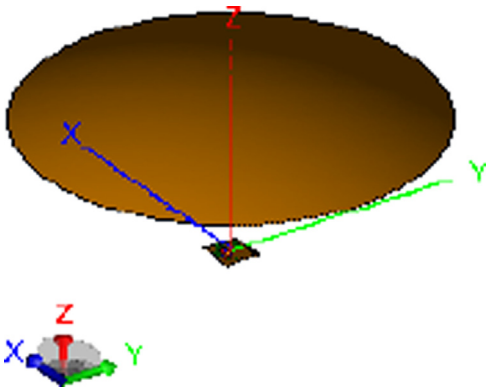


**Fig. 7.** CAD view of the feed and of the conductive surface of the reflector. The dielectric structure is not modelled in this analysis.

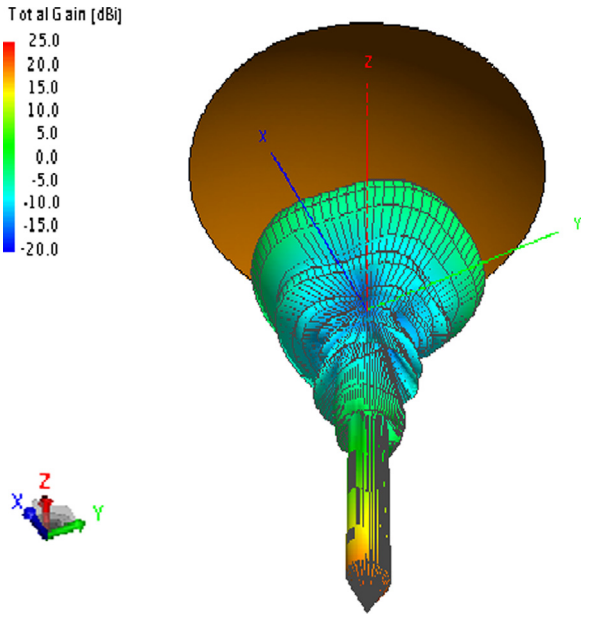


**Fig. 8.** 3D view of the radiation diagram for the patch antenna and the parabolic reflector (2.4 GHz).

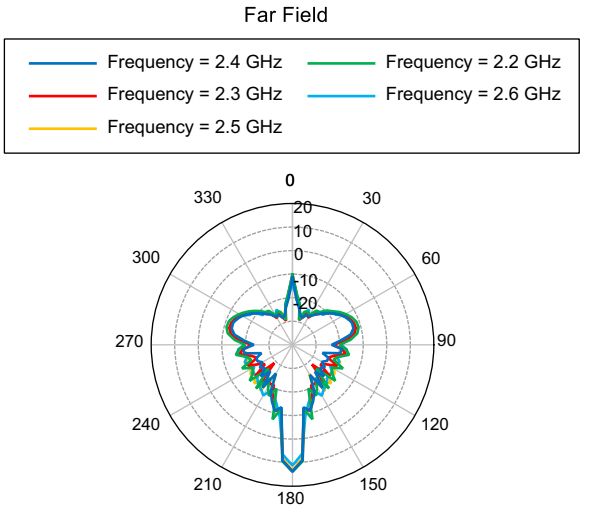


**Fig. 9.** Polar diagram of the radiation of the inflatable antenna (different frequencies).

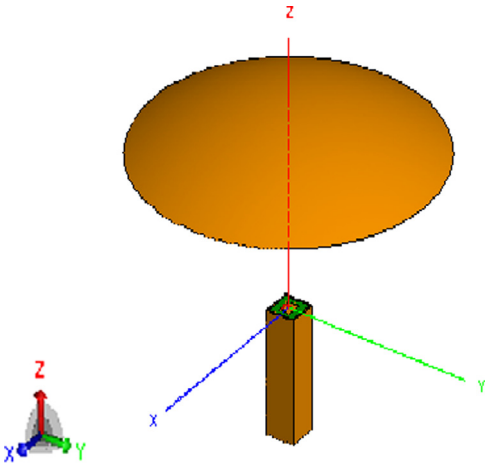


**Fig. 10.** CAD model of the feed mounted on the CubeSat structure together with the parabolic reflector.

CubeSat. The reflector is modelled as a parabolic shape of 0.5 m diameter, 0.5 m focal distance and 1 m distance from the feed (Fig. 7). The material for the reflector is simply modelled as a perfect electric conductor, which is accurate enough for the purpose of this analysis. The 3D radiation diagram (at 2.4 GHz) in Fig. 8 and the polar diagram in Fig. 9 show that the parabolic shape acts as a proper reflector. The antenna achieves a narrow radiation pattern with a peak gain of approximately 23 dB. This result is important, since it shows that the non-traditional choice of using a patch antenna and not a horn as the feed for the antenna does not negatively affect the radiation diagram of the parabolic reflector (with the exception of some side lobes due to spillover losses).

The analysis with the CubeSat structure aims to verify that the structure does not affect the radiation pattern. A 3U CubeSat structure made of perfect conductive material is added to the model (Fig. 10). The radiation diagram and the polar diagram shown in Fig. 11 and in Fig. 12 are almost identical to the ones obtained without the CubeSat structure.

The final analysis aims to study the effect of the dielectric. A cone or a cylinder of dielectric are added in the CADFEKO model as shown in Figs. 13 and 14. Due to the extremely high computational complexity of this calculation, the model is run at only one frequency at a time. In this article, only the results computed at 2.4 GHz are included. The results for the cone configuration at 2.4 GHz are shown in Fig. 15 and 16. It can be noticed that the mylar structure attenuates the radiation. The shape becomes more rounded and the peak gain is strongly reduced (now it is 16 dB). The cause for the degradation in the radiation diagram is mostly due to reflections generated by the inclination of the conical shape with respect to the direction of the electromagnetic rays. In fact,

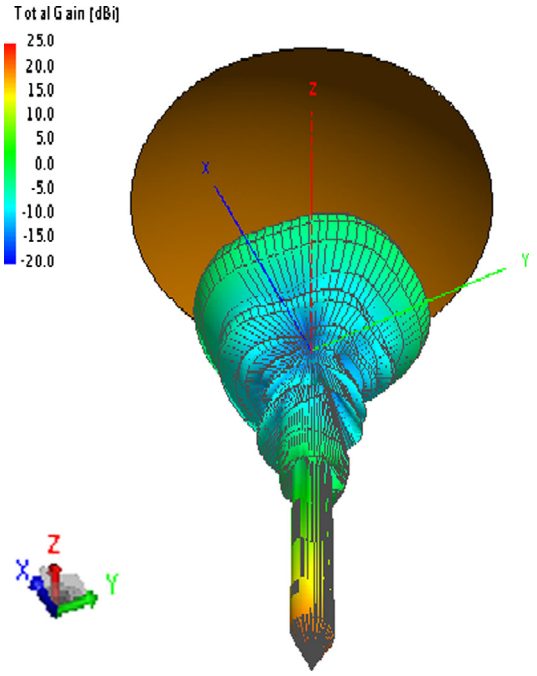


**Fig. 11.** Radiation diagram for the parabolic reflector with the feed mounted on the CubeSat structure (3D view, 2.4 GHz). The radiation diagram obtained is almost identical to the one computed without the CubeSat structure.

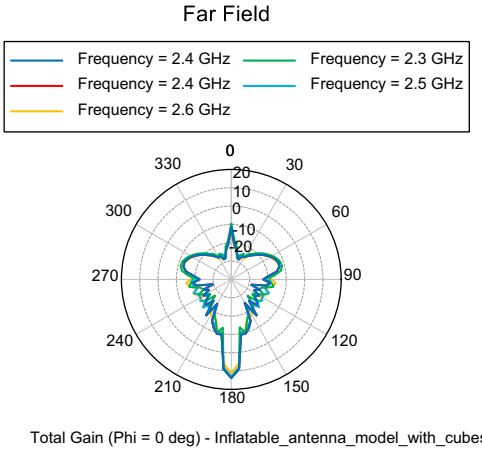


**Fig. 12.** Polar diagram for the parabolic inflatable reflector with the feed mounted on the CubeSat structure. The radiation diagram obtained is almost identical to the one computed without the CubeSat structure.

the cylindrical geometry, which is parallel to the electromagnetic rays, achieves a better result as it is shown in Figs. 17 and 18. In this case, the shape of the radiation resembles the one obtained without the dielectric (Figs. 8, 9, 11, and 12) and the peak gain is approximately 21 dB, very close to the 23 dB obtained without the dielectric (Fig. 11).

In conclusion, the analysis reveals that:

1. The microstrip patch antenna is an appropriate choice as the feed for the inflatable antenna. The dimensions, the focal distance, and the location of the parabolic reflector allow the inflatable antenna to achieve a peak gain of approximately 23 dB (at 2.4 GHz) without dielectric.
2. The CubeSat shape does not affect the radiation.
3. The dielectric inflatable structure has effects on the radiation shape and on the peak gain. The conical shape generates a more rounded radiation pattern and strongly reduces the peak gain (16 dB), while the cylindrical shape generates a radiation pattern which is similar to the one modeled without the dielectric. In this last case, the peak gain is only reduced by 2 dB (21 dB). Hence, according to the radiation analysis, the cylindrical configuration is the preferred choice.

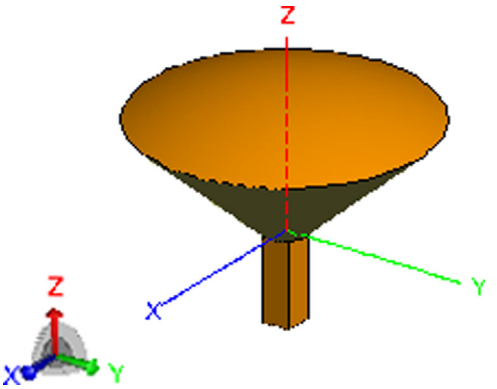


**Fig. 13.** CAD model of the inflatable antenna with the dielectric structure modelled in a conical shape.

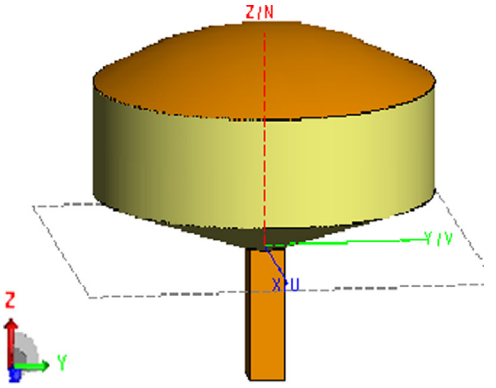


**Fig. 14.** CAD model of the inflatable antenna with the dielectric structure modelled in a cylindrical shape.

The next section will provide details on the micrometeoroid analysis performed.

### 3.3. Micrometeoroid threat and leak rate analysis

Micrometeoroid impacts with the inflated antenna are unavoidable; however, by choosing the right sublimating powders, the lifetime of the satellite can extend for many years even though the antenna is riddled with holes from micrometeoroid impacts.

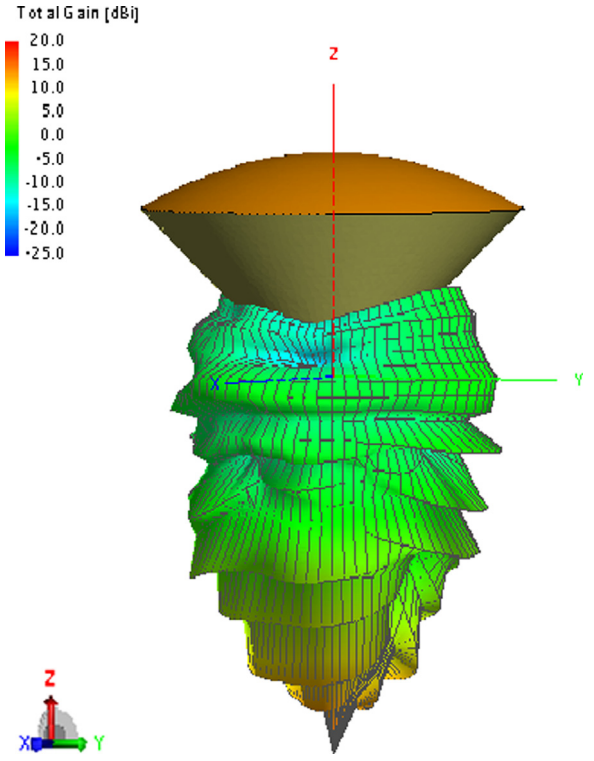


**Fig. 15.** Radiation model (2.4 GHz) of the inflatable antenna mounted on an inflatable conical dielectric shape (3D view).

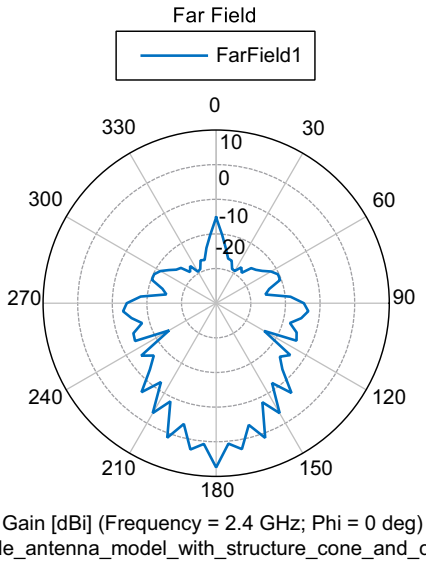


al Gain [dBi] (Frequency = 2.4 GHz; Phi = 0 deg) - Inflatable_antenna_model_with_structure_cone_and_cubesat

**Fig. 16.** Polar diagram (2.4 GHz) of the inflatable antenna mounted on an inflatable conical dielectric shape. A reduction of the peak gain can be observed.

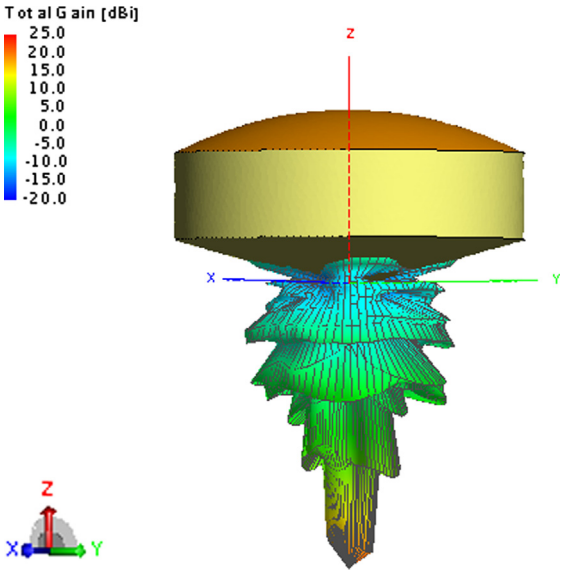


**Fig. 17.** Radiation model (2.4 GHz) of the inflatable antenna mounted on an inflatable cylindrical dielectric shape (3D view).

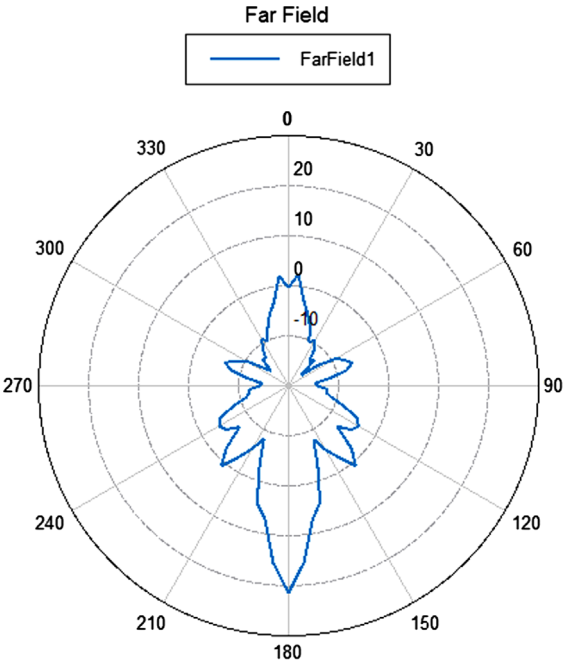


Total Gain [dBi] (Frequency = 2.4 GHz; Phi = 0 deg) - Inflatable_antenna_model_with_structure

**Fig. 18.** Polar diagram (2.4 GHz) of the inflatable antenna mounted on an inflatable cylindrical dielectric shape. The peak gain is close to the one obtained without the dielectric.

The SPENVIS [13] program was used to estimate the flux of micrometeoroids at orbital altitudes of 370 km, 650 km, and 2000 km (SPENVIS does not compute fluxes for geosynchronous orbit, so the highest altitude was used as an approximation for geosynchronous orbit). The micrometeoroid flux does not change appreciably between these three orbits, so only the flux at 370 km is considered for a first-order analysis of the micrometeoroid threat (Fig. 19).

The penetration depth of micrometeoroids moving at 15 km/s through Mylar is 16.8 μm [2], which was enough to penetrate the Echo 1 and 2 balloons since the Mylar

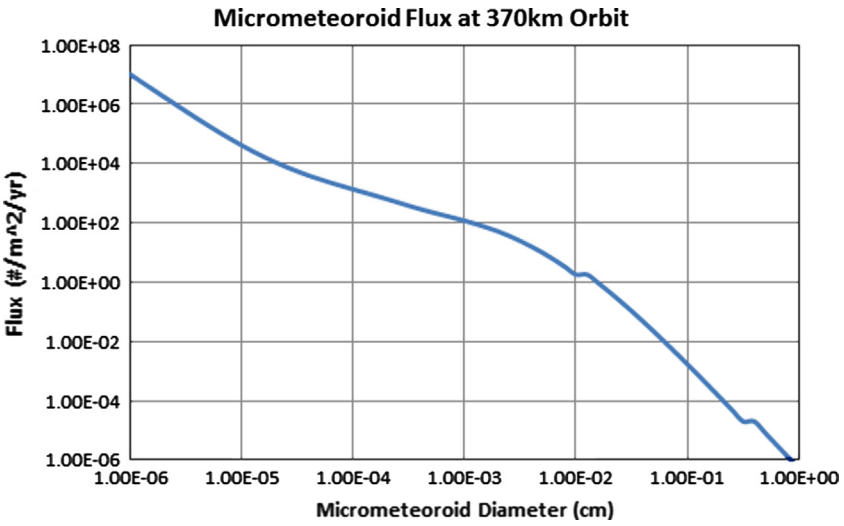


**Fig. 19.** SPENVIS model of the micrometeoroid flux at an orbital altitude of 370 km.

thickness was 12.8 μm. However, SPEVNIS only gives the number flux and not the distribution of energies, so a substantial percentage of micrometeoroids will still penetrate the thicker inflatable antenna, possibly going through both sides. The flux of micrometeoroids larger than 10 μm in diameter is 117 per square meter per year. At its widest, the antenna has a projected area of 0.785 $m^2$, so the antenna would receive approximately 92 impacts of this size or greater per year, resulting in 184 small holes if the micrometeoroids penetrate both sides.

These holes can be modelled as miniature ideal vacuum pumps with a volumetric flow rate of:

$$Q_{out}^{ideal} = \frac{\bar{c}A}{4} = \frac{A(t)}{4}\sqrt{\frac{8kT}{\pi m}} \tag{2}$$

where $A$ is the combined area of holes created by impacts, $\bar{c}$ is the mean molecular speed of molecules, $k$ is Boltzmann's constant, $T$ is the temperature in Kelvin, and $m$ is the molecular mass in kg. This can be converted to a mass flow rate with:

$$\dot{m} = \rho Q_{out}^{ideal} = \frac{p}{RT} Q_{out}^{ideal} \tag{3}$$

where $\rho$ is the density of the sublimated gas, $p$ is the gas at its vapour pressure, and $R$ is the gas constant. From this, information, a model can be built to determine the operational lifetime of the satellite before the supply of sublimating powder runs out and the antenna can no longer support its shape.

An additional consideration for the lifetime of the antenna is the vapour pressure of the sublimating powder and the thermal environment it is in – most potential materials' vapour pressures vary logarithmically with temperature according to:

$$\log \rho_v = A - \frac{B}{T + C} \tag{4}$$

where $A$, $B$, and $C$ are constants and $p_v$ is the vapour pressure. At higher pressures, the mass flow rate is higher so the lifetime is shorter.

Assume that the antenna has 100 holes in it each 10 μm in diameter (as would be expected after a year or so of operation), that benzoic acid is being used at the sublimating powder, and the orbital temperature is a constant 373 K. With only 1 g of benzoic acid, the antenna will stay inflated for 1.22 years. If the Mylar is thick enough to resist some impacts, the lifetime would be ever greater.

Another possibility to extend mission lifetime is to use dual sublimating powders. One would have a higher vapour pressure than the other and be most effective in deploying and inflating the satellite once it is on orbit, but it would quickly leak out and sublimate away when the antenna was hit by micrometeoroids. The second sublimating powder would have a lower vapour pressure but still provide enough force to counteract environmental pressures like solar pressure and drag.

The use of layers of protective material such as Kevlar was considered to prevent micrometeoroid impacts, but the extra mass would be prohibitive, its presence would interfere with signal transmission, and fabrication and packing would be even more difficult.

Additional modelling of the thermal environment of the inflatable is crucial to predicting the internal pressure of the antenna because the potential sublimating powders' vapour pressures vary logarithmically with temperature. Since mass flow rate is directly proportional to pressure, the maximum operable lifetime of the antenna is also related to the temperature and initial mass of sublimating powder. Finally, the internal pressure also affects dynamic control and pointing stability since there is no rigid connection between the satellite and the reflector.

### 3.4. Control and pointing

The inflatable antenna will need to be pointed accurately at the receiving ground station(s). Before choosing a control system to point the antenna and maintain three-axis control, the torque environment for a variety of orbits was analyzed.

SolidWorks was used to obtain an inertia matrix for both the cylindrical antenna configuration and the conical antenna configuration. Then, a series of circular orbits from 300 km to 37,786 (geostationary orbit) were considered. The aerodynamic drag torque, gravity gradient torque and solar radiation pressure torque were analyzed. The magnetic torque was not considered in this analysis because the early development stage of the spacecraft bus and specific components does not allow for a good estimation of the residual magnetic moment. Care will be taken as the design progresses to minimize the spacecraft's residual magnetic moment.

Table 2 lists the assumptions made in the torque calculations. An effort was made to consider worst-case parameters since accurate values are not yet available.

Using the parameters listed above, environmental torques were calculated and the results are shown in Fig. 20.

**Table 2**
Parameters used to calculate environmental torques on inflatable antenna. Orbit altitude ranged from 300 km to 37,786 km (geostationary orbit). Moments of inertia were calculated from the CAD models shown in Figs. 13 and 14. $C_{pa}$ is the centre of pressure for the purpose of drag calculations, $c_{ps}$ is the centre of pressure for the purpose of radiation pressure calculations.

| Parameter | Value | |
|---|---|---|
| | Cylinder | Cone |
| Mass (kg) | 4.54 | 4.32 |
| $I_x$ (kg m$^2$) | 0.16 | 0.09 |
| $I_y$, $I_z$ (kg m$^2$) | 0.27 | 0.24 |
| Coefficient of drag | 2.5 | 2.5 |
| $\|c_{pa}-cg\|$ (m) | 0.1 | 0.1 |
| $\|c_{ps}-cg\|$ (m) | 0.2 | 0.2 |
| Effective surface area (m$^2$) | 2.5 | 2 |
| Reflectance coefficient | 0.5 | 0.5 |
| Orbit eccentricity (deg.) | 0 | 0 |
| x-axis offset (max) from local vertical (deg.) | 30 | 30 |

At very low altitudes, drag torque is dominant. Between 600 and 800 km, radiation pressure becomes the dominant torque. These calculations indicate that very low orbits ( $<500$ km) will not be acceptable for the inflatable antenna spacecraft. A technology demonstration mission could be flown at an altitude of 600–700 km. This orbital altitude is well within the reach of current CubeSat-bearing launch vehicles and should allow a variety of launch opportunities.

The torque calculations in this early stage of the design process indicate that a commercially available reaction wheel-based control system will provide adequate pointing for the inflatable antenna. The pointing performance requirement is set by the angular size of the antenna's half-power beam width. For S-band, the HPBW is approximately 8.75°. As shown in Fig. 18, the real beamwidth of the antenna may be slightly wider due to the effects of the dielectric mylar that forms the conical/cylindrical structure of the antenna.

The current baseline ADCS system is the MAI-400 from Maryland Aerospace. Each MAI-400 reaction wheel can provide 0.625 mNm of torque [14]. As shown in Fig. 20, the radiation pressure torque for the cylindrical antenna configuration is approximately 3.5 μNm (constant for all altitudes). The MAI-400 has ample torque capacity to counter this and other environmental torques that the spacecraft will experience. Based on previous simulations of MAI-400 performance for MIT's ExoplanetSat, pointing precision of 1° is achievable [15]. There is therefore a large margin on the pointing performance of the inflatable antenna CubeSat.

Attitude sensing will be provided by sun sensors and gyros mounted to the solar panels and a magnetometer mounted to the flight computer board. A miniature star tracker (manufactured by Sinclair Interplanetary [16]) may be added to the sensor suite if future simulations indicate that the sun sensors, gyros, and magnetometer cannot provide a satisfactory attitude estimate.

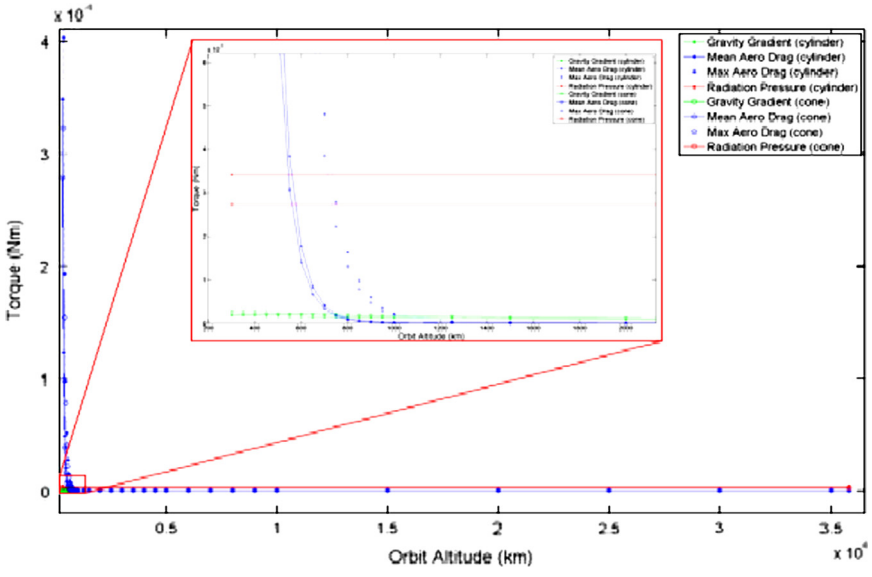


**Fig. 20.** Torque calculations for both cylindrical and conical antenna configurations. Red inset box shows region where radiation pressure torque begins to dominate drag and gravity gradient torques.

A full ADCS simulation for the inflatable antenna CubeSat is underway and will be reported in a future work. This paper also does not consider internal torques and dynamics induced as the spacecraft slews. These will be the topic of a future work.

### 3.5. Spacecraft design and deployment mechanism

The inflatable antenna prototype will be flown on a 3-unit ($10 \times 10 \times 30$ cm$^3$) CubeSat, leveraging the growing body of commercial off-the-shelf CubeSat components wherever possible. Trade studies are currently underway to choose components from several CubeSat vendors.

The antenna and deployment system will fill approximately half of a CubeSat unit ($10 \times 10 \times 5$ cm$^3$). The vacuum-packed antenna will be held between a spring-loaded patch antenna and the end face covering plate (Fig. 21). Upon deployment from the PPOD, burn-through resistors will release the end face covering. The spring will push the patch antenna and inflatable material outwards until the patch antenna reaches the end of the CubeSat body. Sublimating powder will then allow the deployed antenna to inflate (see Section 3.1). The deployment process will be recorded by a small camera located on the upper corner of the patch antenna (Fig. 21).

The remaining spacecraft volume will hold the avionics board, electric power system (EPS), batteries, transceiver, back-up patch antenna, and attitude control system, all of which will be purchased from CubeSat or other space system vendors (Fig. 22).

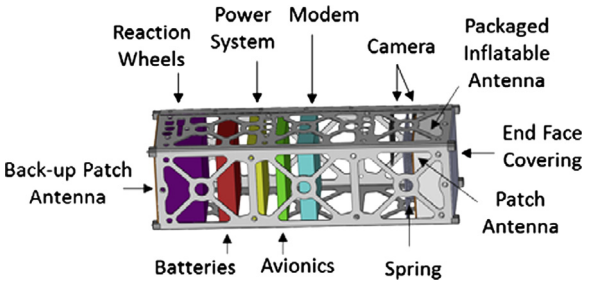


**Fig. 21.** Schematic of the spacecraft before the antenna is deployed. The component volume estimates are based on commercial parts. The body-mounted solar panels, on the long sides of the spacecraft, are not shown.

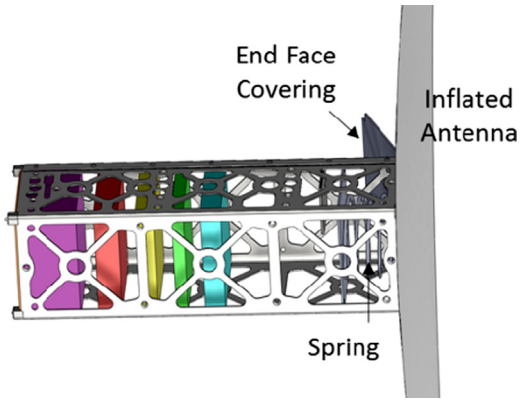


**Fig. 22.** Schematic of the spacecraft after the antenna is deployed. The component volume estimates are based on commercial parts. The body-mounted solar panels, on the long sides of the spacecraft, are not shown.

The avionics board will have a PC/104 form factor compatible with the CubeSat structure, and will have at least 2 GB of data storage to accommodate rapid imaging during the antenna deployment process. The avionics board will include a 32-bit microprocessor with I$^2$C interfaces.

In order to point the inflatable antenna, the MAI-400 reaction wheel unit will be used to orient the spacecraft. The MAI-400 was chosen based on its pointing precision (60″) and heritage from MIT/Draper ExoplanetSat mission.

The transceiver and patch antenna will ensure communication with the spacecraft prior to the deployment of the inflatable antenna, and will continue to be used if the inflatable antenna fails to deploy. The back-up antenna will be identical to the patch antenna used in the main inflatable system. It will be mounted on the opposite end of the CubeSat structure (see the left hand side of Fig. 21). The Open System for Agile Ground Stations (OSAGS) and on-campus MIT ground stations are both under consideration as possible ground station candidates.

The power system will consist of an EPS board, batteries, and four body-mounted solar panels placed along the $10 \times 30$ cm$^2$ sides of the CubeSat. The EPS will provide the necessary power to each subsystem component at the proper voltage. It must be able to interface with at least four solar panels, manage the charging of lithium ion batteries, use I$^2$C interfaces, and contain both 3.3 V and 5 V outputs. The batteries must hold at least 30 Wh of energy, and use an I$^2$C interface. The batteries and EPS will be purchased from the same company to ease integration. Four solar panels, each with 6–7 solar cells, will be mounted on the spacecraft sides.

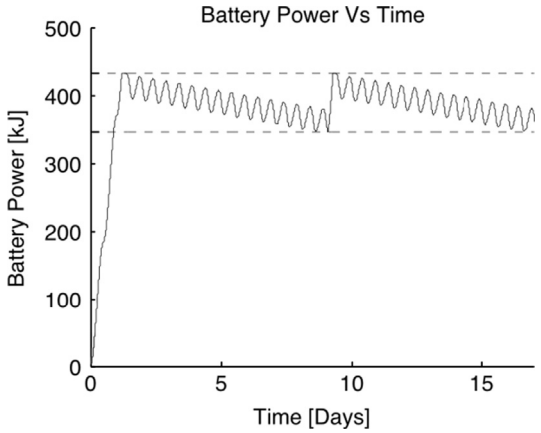


**Fig. 23.** Baseline battery power as a function of time. The lower dashed line represents the lower power limit of four 30 Wh batteries, assuming a depth of discharge of 20%. The upper line represents the maximum battery power of four 30 Wh batteries. During the initial power-up phase and when charging from battery minima to maxima, the transceiver is in receiving mode only (~1 W). When discharging the battery, the transceiver is in transmitting mode (~5.5 W).

Simulations of power provided by the solar panels in a geosynchronous orbit are shown in Fig. 23. The component power consumptions are taken from GomSpace [17] parts. During the initial power-up phase, the avionics and EPS only are drawing power from the batteries. After the batteries have reached their maximum energy capacity and the inflatable antenna has deployed, the transceiver will begin transmitting telemetry and image data. When the battery energy reaches its lower limit, based on a depth of discharge of 20%, the transceiver will enter receiving mode, and will not transmit until the batteries have again reached their maximum energy levels. While the transceiver can enter receiving mode at any time after the initial power-up phase, this power budget represents the most conservative model.

## 4. Test plan

To validate the design and to fully characterize the radiation of the antenna, as well as the deployment mechanism and the inflation process, a series of tests need to be performed. Specifically, the tests currently planned are listed as follows:

- Anechoic chamber test: This test will be used to measure the radiation pattern of the antenna. Specifically, the antenna will be attached to the CubeSat structure and to the patch antenna feed. Then, the antenna will be inflated with air and the radiation pattern will be modeled on the horizontal and on the vertical axis. Multiple patch antenna feeds will also be tested and the effects of the dielectric cone or cylinder on the radiation pattern will be measured.
- Vacuum chamber test: This test will be used to validate the deployment and the inflation mechanism performed with the use of the sublimating powder. This test will reveal eventual challenges and unexpected issues in the dynamic of the deployment. Additionally, to prepare for the test, the team will need to properly fold and pack the antenna in the CubeSat canister trying to minimize the residual air.
- Thermal vacuum chamber test: The effect of the change of temperature on the inflated dish will be measured and eventual deformations of the shape will be included in the updated version of the radiation model.
- Micrometeoroid test: The endurance of the inflatable structure will be tested with respect to meteoroid impacts. Specifically, the reflector will be hit by particles of similar size and energy of the possible micrometeoroids. The results will provide clues on how likely micrometeoroid impacts can affect the shape of the reflector.

## 5. Conclusions

The article describes the recent progress in the development of an inflatable antenna for CubeSats. An overview of the benefits for developing this technology is presented. Details on the antenna design, on the simulation of the radiation and on other aspects of the spacecraft design are described. Finally, the set of environmental tests that will be performed are listed.

Future work will include the final construction of the prototype and the performance of the related tests.

## References

[1] Stefano Speretta, et al., Nanosatellite Communication System Trends, in: Proceedings of the 62nd International Astronautical Conference, Cape Town, 2011.
[2] R.E. Freeland, et al., Inflatable Deployable Space Structures Technology Summary, in: Proceedings of the 49th International Astronautical Conference, 1998.
[3] R.E. Freeland, G.D. Bilyeu, In-step inflatable antenna experiment, Acta. Astronaut. 30 (1993) 29–40.
[4] R.E. Freeland, G.D. Bilyeu, G.R. Veal, Development of flight hardware for a large, inflatable-deployable antenna experiment, Acta. Astronaut. 38 (1996) 251–260.
[5] R.E. Freeland, et al., Large inflatable deployable antenna flight experiment results, Acta. Astronaut. 41 (1997) 267–277.
[6] David P. Cadogan, John K. Lin, Mark S. Grahne, The development of inflatable space radar reflectarrays, йил, in: Proceedings of the 40th AIAA/ASME/ASCE/AHS/ASC Structures, Structural Dynamics, and Materials Conference 1999.
[7] John K. Lin et al., An inflatable microstrip reflectarray concept for Ka-band applications, йил, in: Proceedings of the 41st AIAA/ASME/ASCE/AHS/ASC Structures, Structural Dynamics, and Materials Conference, 2000.
[8] John K. Lin, et al., Advanced precipitation radar antenna singly curved parabolic antenna reflector devleopment, AIAA 1651 (2003) 1–10.
[9] John K. Lin et al., Concept study of a 35-m spherical reflector system for NEXRAD in space application, йил, in:Proceedings of the 47th AIAA/ASME/ASCE/AHS/ASC Structures, Structural Dynamics, and Materials Conference, 2006.
[10] Xu, Yan, Fu-Ling Guan, Structure design and mechanical measurement of inflatable antenna, Acta. Astronaut. 76 (2012) 13–25.
[11] A. Babuscia et al., Inflatable antenna for cubesat: motivation for development and initial trade study, in: Proceedings of the First Interplanetary CubeSat Workshop, Cambridge, 2012.
[12] FEKO, [Online] ⟨http:/www.feko.info/⟩ (accessed 24.08.12).
[13] SPENVIS, [Online] ⟨http:/www.spenvis.oma.be/⟩(accessed 6.09.2012).
[14] Maryland Aerospace. The 1/2U MAI-400 A La Carte Spec Sheet. www.miniADACS.com, [Online] ⟨http:/www.miniadacs.com/linked/2012-04-27%20mai-400%20a%20la%20carte%20specification.pdf⟩.
[15] Chris Pong, et al., Achieving high-precision pointing on Exoplanet-Sat: Initial feasibility analysis, SPIE Proc. 7731 (2010).
[16] Sinclair Interplanetary, [Online], Startrackers, ⟨www.sinclairinterplanetary.com⟩.
[17] Gomspace, [Online] ⟨http:/www.gomspace.com/⟩ (accessed 24.08.12).